JOURNAL OF Materials CHEMISTRY

Incommensurate phases in the Ba–Mn–Pd–O system

Peter D. Battle,*[a] Jonathan C. Burley,[a] Edmund J. Cussen,[a] Jacques Darriet[b] and François Weill[b]

[a]*Inorganic Chemistry Laboratory, Oxford University, South Parks Road, Oxford, UK OX1 3QR. E-mail: peter.battle@chem.ox.ac.uk*
[b]*ICMCB, Château Brivazac, Av. Dr. Schweitzer, 33608 Pessac Cedex, France*

Received 29th July 1998, Accepted 7th December 1998

Polycrystalline samples of bulk composition $Ba_5Mn_3PdO_{12}$, $Ba_6Mn_4PdO_{15}$, and $Ba_7Mn_5PdO_{18}$ have been synthesised and characterised by X-ray diffraction, electron diffraction and magnetometry. These compounds adopt a 2H-related crystal structure consisting of [001] chains of MnO_6 and PdO_6 polyhedra, with Ba^{2+} cations separating the chains. The three compounds, each of which is commensurate in the *xy* plane but incommensurate along the *z* axis, differ in the ratio of octahedra to trigonal prisms in the chains (3 : 1, 4 : 1 and 5 : 1 respectively). The lattice parameters of the four dimensional trigonal unit cell are typically $a \approx 10.02$ Å, $c_1 \approx 4.3$ Å, $c_2 \approx 2.61$ Å. The homogeneity and crystallinity of the samples increases with the ratio of octahedra to trigonal prisms and is greater in the *xy* plane than parallel to *z*. The magnetic susceptibility of all three phases deviates from the Curie–Weiss law below 100 K, but no magnetic phase transition is apparent above 5 K.

Introduction

Recent research by a number of different groups[1–10] has lead to the recognition of a new family of mixed metal oxides which was initially assigned the general formula $A_{3n+3}A'_nB_{n+3}O_{6n+9}$.[11] These compounds can be considered to provide a link between the 2H perovskite structure of $BaNiO_3$[12] and the Sr_4PtO_6 structure.[13] The former consists of infinite chains of face-sharing NiO_6 octahedra parallel to *z*, with the interchain space occupied by Ba^{2+} cations, whereas the latter consists of chains made up of alternating PtO_6 octahedra and SrO_6 trigonal prisms, also linked by face-sharing, and with the interchain space occupied by the remaining Sr^{2+} cations. $BaNiO_3$ can be described by the formula $A_{3n+3}A'_nB_{n+3}O_{6n+9}$ with $n=0$, and Sr_4PtO_6 (A = A′ = Sr) is the $n=\infty$ member of the same series. It is also possible to describe 2H $BaNiO_3$ as comprising an hcp arrangement of pseudo close-packed layers, each of composition BaO_3, with Ni^{2+} occupying the octahedral, 6-coordinate interstices formed between the layers. In order to extend this type of model to include Sr_4PtO_6 it is necessary to introduce anion vacancies into every layer, thus modifying their stoichiometry to A_3O_6. Hcp stacking of these layers generates two types of 6-coordinate interstitial site which are coordinated by oxide ions. Octahedral sites are again found centred between the layers, but trigonal prismatic sites, centred within the A_3O_6 layers, are also created (Fig. 1). These are relatively large and are denoted A′ in the general formula given above. The composition of a layer having an occupied A′ site can thus be written $A_3A'O_6$. The members of the series with $0<n<\infty$ consist of a periodic but mixed stacking of AO_3 ($=A_3O_9$) and $A_3A'O_6$ layers, with the interlayer interstices occupied by a transition metal cation, B. This results in chains parallel to *z* with a ratio of octahedra (o) to prisms (p) which depends on the value of *n*. $Ba_6CuIr_4O_{15}$[2] and $Sr_4Ni_3O_9$[14] are examples of members of the series having $n=1$ and 3 respectively; the corresponding values of the ratio o : p are 4 : 1 and 2 : 1. The general formula of these compounds can be written as $(A_3A'O_6)_n(A_3O_9)$, a notation which emphasises that the structural framework can be described as a stack of two different layer types, with an A_3O_9 layer being inserted after every *n* anion-deficient layers. Consideration of this description facilitates recognition of the possibility of inserting more than one A_3O_9 layer, that is moving to the formula $(A_3A'O_6)_n(A_3O_9)_m$ with $m \geq 1$, or even to an extended repeating unit, for example $(A_3A'O_6)_n(A_3O_9)_m(A_3A'O_6)_p(A_3O_9)_q$.[15]

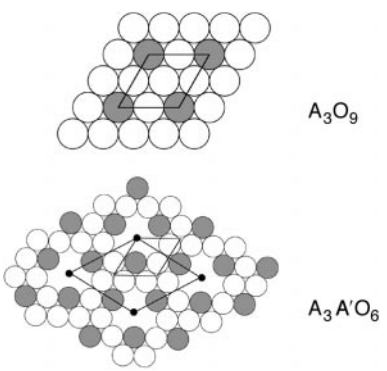

Fig. 1 A_3O_9 and $A_3A'O_6$ layers. The unit cells of both layer types are shown, with $a'=\sqrt{3}a$. Shaded circles, A; black circles A′; empty circles, O.

Interest in these compounds is high because of the possibility that they will show unusual 1D electronic properties.[9,16] Strong cation–cation interactions are expected along a chain of face-sharing octahedra, but the greater cation–cation separation around a prismatic site will weaken the interactions. It should therefore be possible to control the electronic properties of a compound by varying the o : p ratio in the chains. It may also be possible to exercise a degree of control by careful choice of the A′ cation which occupies the prismatic sites. Having previously elucidated the range of structures available,[15] we have now introduced Pd^{2+} into the prismatic site. There were a number of reasons for this choice of element. Earlier studies[2,8,17,18] have shown that compounds in this family are relatively easy to prepare when $A'=Cu^{2+}$, and that the Cu^{2+} cations often move away from the centre of the trigonal prisms towards one of the rectangular faces. They thus move from a 6-coordinate site towards a 4-coordinate site, perhaps driven by the degeneracy of the $3d^9$ ground state. We believed that if the structure is stabilized by an A′ cation which can take 4-coordination, then the introduction of Pd^{2+} was likely to lead to the formation of new phases. It would also place a cation with partially occupied, relatively extensive 4d orbitals on the larger cation site in the chains, thus enhancing the cation–cation interactions around this site. However, before the experiments were undertaken, it was not clear whether the structural changes necessitated by the increased size of Pd^{2+} relative to Cu^{2+} would allow this idealised scenario to be

realised. The synthesis, structural chemistry and magnetic properties of three new Pd-containing compositions, $Ba_5Mn_3PdO_{12}$, $Ba_6Mn_4PdO_{15}$ and $Ba_7Mn_5PdO_{18}$, are described below. These stoichiometries were selected for this exploratory work because their crystal structures (Fig. 2) are predicted[15] to contain [001] chains with increasing o : p ratios (3 : 1, 4 : 1 and 5 : 1 respectively). $Ba_6Mn_4PdO_{15}$, with a total of 6 layers per unit cell, can be described by the formula $(A_3A'O_6)_n(A_3O_9)$ with $n=1$, but the other two compositions lie beyond this simple formulation. They have a total of either 10 ($Ba_5Mn_3PdO_{12}$) or 14 ($Ba_7Mn_5PdO_{18}$) layers per unit cell, and can be described in the notation developed previously[17] as $(p, q)=(5, 8)$ and $(7, 12)$ respectively.

Experimental

Polycrystalline samples of overall composition $Ba_5Mn_3PdO_{12}$, $Ba_6Mn_4PdO_{15}$ and $Ba_7Mn_5PdO_{18}$ were prepared by firing alumina crucibles containing intimately ground, stoichiometric quantities of $BaCO_3$, Pd metal and MnO_2 in air. All the reaction mixtures were initially heated for $\approx$12 h at 800 °C and $Ba_5Mn_3PdO_{12}$ was then fired at 1200 °C for 8 days, $Ba_6Mn_4PdO_{15}$ at 1200 °C for 20.8 hours, and $Ba_7Mn_5PdO_{18}$ at 1000 °C for 43 hours and at 1200 °C for 228 hours. X-Ray powder diffraction patterns of the reaction products were collected using a Siemens D5000 powder diffractometer operating in Bragg–Brentano geometry with Cu-Kα_1 radiation. A step size $\Delta 2\theta = 0.02°$ was used. Electron diffraction patterns were obtained using a JEOL 2000FX microscope operating at 200 kV. An alcohol suspension of the compound was prepared, and a drop of this suspension was deposited on a holey-carbon-supported grid. A Quantum Design MPMS 5000 SQUID magnetometer was used to make magnetic susceptibility measurements in fields of 100 G and 1000 G after cooling in the absence of a field (ZFC) and after cooling in the measuring field (FC).

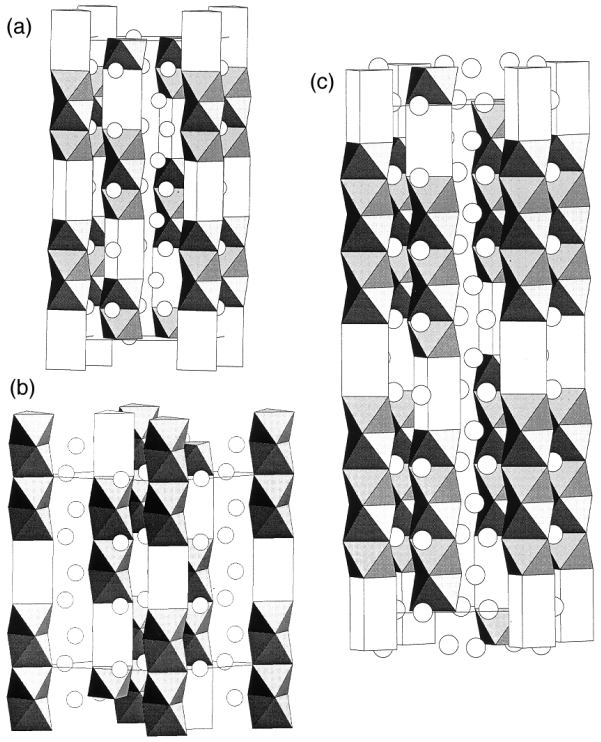

Fig. 2 Idealised crystal structures of (a) $Ba_5Mn_3PdO_{12}$, (b) $Ba_6Mn_4PdO_{15}$ and (c) $Ba_7Mn_5PdO_{18}$. Alternative structures with different relative displacements of the 3 chains within the unit cell are possible, but the o : p sequence within the chains is invariant.

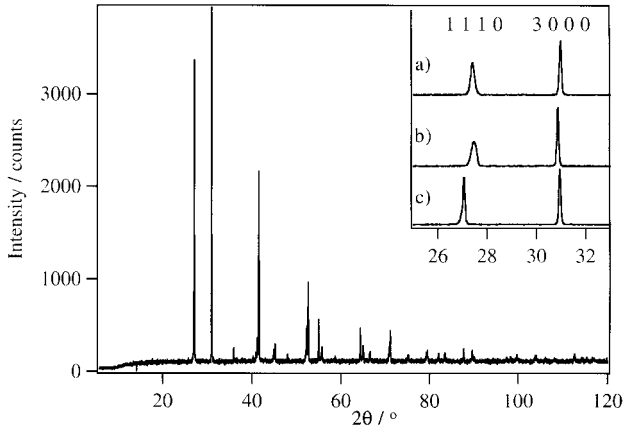

Fig. 3 X-Ray powder diffraction pattern of $Ba_7Mn_5PdO_{18}$. The inset shows relative peak broadening in a) $Ba_5Mn_3PdO_{12}$, b) $Ba_6Mn_4PdO_{15}$ and c) $Ba_7Mn_5PdO_{18}$.

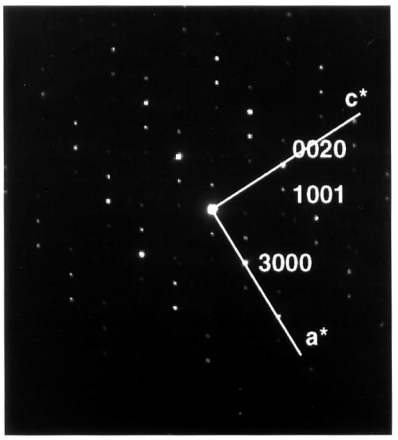

Fig. 4 [010] Electron diffraction pattern of $Ba_5Mn_3PdO_{12}$.

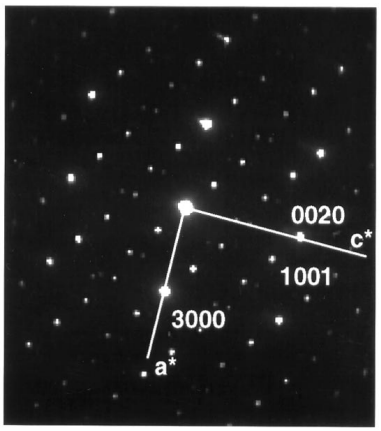

Fig. 5 [010] Electron diffraction pattern of $Ba_6Mn_4PdO_{15}$.

Results

The X-ray powder diffraction patterns of all three reaction products resembled those expected for the anticipated trigonal crystal structures, with no evidence for the presence of impurity phases. However, it proved impossible to index the patterns using a three dimensional unit cell. In order to achieve a satisfactory level of agreement between observed and calculated *d*-spacings it was necessary to treat all three of the oxides as composite crystals, and to index the data in terms of 4 Miller indices $\{hklm\}$, corresponding to the unit cell parameters a, b $(=a)$, c_1, and c_2. This strategy has been described in detail in our earlier publications.[2,15,17] The refined unit cell parameters are summarised in Table 1. The full width at half

Table 1 Unit cell parameters of $Ba_5Mn_3PdO_{12}$, $Ba_6Mn_4PdO_{15}$ and $Ba_7Mn_5PdO_{18}$ derived from X-ray powder diffraction data

Compound	a/Å	c_1/Å	c_2/Å	c_1/c_2
$Ba_5Mn_3PdO_{12}$	10.044(6)	4.315(23)	2.597(2)	1.661
$Ba_6Mn_4PdO_{15}$	10.020(7)	4.251(5)	2.616(5)	1.625
$Ba_7Mn_5PdO_{18}$	10.002(4)	4.386(5)	2.564(3)	1.711

maximum (FWHM) of the Bragg peaks of $Ba_5Mn_3PdO_{12}$ was unusually large, and this sample can be regarded as poorly crystalline over the distance scale sampled in an X-ray experiment. It was noticable that the FWHM generally decreased with increasing Ba : Pd ratio, approaching the instrumental resolution ($\approx 0.08^\circ$ 2θ) for some peaks in the pattern of $Ba_7Mn_5PdO_{18}$ (Fig. 3). In any particular pattern, the $\{hk00\}$ peaks were narrower than $\{hkl0\}$ or $\{hk0m\}$, as illustrated by the data in Table 2.

All the crystallites studied in the electron microscope gave diffraction patterns characteristic of 2H-related compounds; we found no evidence for the presence of other structural types. The [010] electron diffraction patterns obtained from $Ba_5Mn_3PdO_{12}$, $Ba_6Mn_4PdO_{15}$ and $Ba_7Mn_5PdO_{18}$ are presented in Fig. 4, 5, and 6 respectively. These patterns are typical of those obtained from compounds belonging to this structural family.[2,19] They can be interpreted either on the basis of a trigonal cell and a modulation vector, or on the basis of two interpenetrating cells of trigonal symmetry having the same basal (a, b) plane but different c parameters, c_1 and c_2. The indexing given on the diffraction patterns uses the latter convention. The c_1/c_2 ratios determined from the electron diffraction patterns are: $Ba_5Mn_3PdO_{12}$, $c_1/c_2 = 1.70$; $Ba_6Mn_4PdO_{15}$, $c_1/c_2 = 1.63$; $Ba_7Mn_5PdO_{18}$; $c_1/c_2 = 1.72$.

None of the magnetic susceptibility data collected on the Pd-containing products showed any hysteresis between ZFC and FC experiments, and no significant field dependence was observed. The inverse ZFC susceptibility of each compound is plotted as a function of temperature in Fig. 7, and the parameters derived by fitting a Curie–Weiss law to the data collected in the temperature range $195 \leqslant T/\mathrm{K} \leq 300$ in a field of 1000 G are listed in Table 3. No magnetic phase transitions are apparent in any of the data sets.

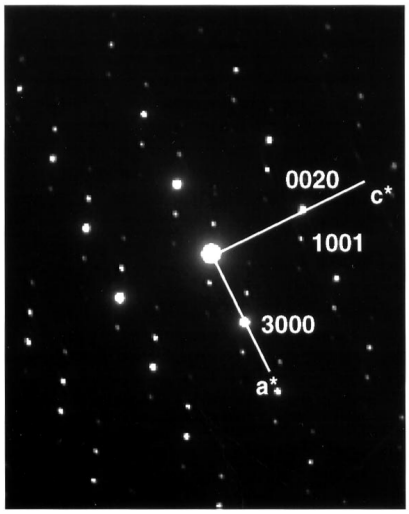

Fig. 6 [010] Electron diffraction pattern of $Ba_7Mn_5PdO_{18}$.

Table 3 Magnetic parameters of $Ba_5Mn_3PdO_{12}$, $Ba_6Mn_4PdO_{15}$ and $Ba_7Mn_5PdO_{18}$

Compound	C_m[a]/cm^3 K mol^{-1}	θ/K
$Ba_5Mn_3PdO_{12}$	5.4(1)	−321(10)
$Ba_6Mn_4PdO_{15}$	8.68(6)	−499(5)
$Ba_7Mn_5PdO_{18}$	10.22(9)	−583(7)

[a]Molar Curie constant derived from high temperature region ($T > 195$ K).

Discussion

The diffraction data presented above show that we have achieved our aim of introducing Pd into this family of compounds. The 6–4–1–15 and 5–3–1–12 stoichiometries have been observed previously in oxides of Ir and Co[2,15,20] but this is the first reported synthesis of the 7–5–1–18 member of this family. However, none of the Pd-containing samples has a commensurate crystal structure. Accounts of related materials[21,22] have ascribed their complex crystallography to a structural mismatch between the transition metal chains and the chains of alkaline earth cations which separate them. Commensurate 6–4–1–15 and 5–3–1–12 compounds have been prepared previously, but incommensuration has been observed in a number of other $(A_3A'O_6)_n(A_3O_9)$ compounds, including 6–4–1–15 phases,[2,4,17] and the results described above perhaps establish this behaviour as the norm rather than the exception; we have suggested previously, on the basis of electron diffraction data, that samples in this family which appear to be commensurate may still adopt modulated structures.

The X-ray diffraction pattern of $Ba_5Mn_3PdO_{12}$ shows peak broadening for all classes of reflection over the full angular range measured. This suggests that the sample is poorly crystalline in all directions, and possibly inhomogeneous. Furthermore, and in contrast to the two samples to be discussed below, there is a significant discrepancy between the c_1/c_2 ratio determined using X-rays (1.661) and that determined using electrons (1.70). This can be explained by assuming that the X-ray data have been indexed to give a mean value for the bulk polycrystalline sample, whereas the use of the electron microscope has resulted in the characterisation of a single crystal in an inhomogeneous sample. Our synthetic procedure should ensure that the bulk composition of the sample is invariant, but it is possible that local variations occur. It is worth noting that the two experimental values of c_1/c_2 lie closer to each other than they do to the ideal commensurate value, which is 1.60 for the structure drawn in Fig. 2.

In contrast to the data from $Ba_5Mn_3PdO_{12}$, the values of the parameter c_1/c_2 derived from X-ray and electron diffraction are in excellent agreement for $Ba_6Mn_4PdO_{15}$ and $Ba_7Mn_5PdO_{18}$. In each case the degree of incommensuration can be gauged by comparing the observed values (1.625, 1.711) with the values expected (1.666, 1.714) for commensurate structures of the appropriate stoichiometry. The value measured in the case of $Ba_6Mn_4PdO_{15}$ differs considerably from

Table 2 X-Ray peak width as a function of $\{hklm\}$ for $Ba_5Mn_3PdO_{12}$, $Ba_6Mn_4PdO_{15}$ and $Ba_7Mn_5PdO_{18}$

Compound	FWHM {1110} 2θ/°	FWHM {3000} 2θ/°	FWHM {2200} 2θ/°	FWHM {2001} 2θ/°
$Ba_5Mn_3PdO_{12}$	0.224	0.154	0.149	0.204
$Ba_6Mn_4PdO_{15}$	0.267	0.090	0.099	0.292
$Ba_7Mn_5PdO_{18}$	0.10	0.08	0.09	0.10

the ideal ratio, but comparable values have been observed previously, for example $c_1/c_2=1.634$ for $Ba_6Ir_4ZnO_{15}$.[2] The range of c_1/c_2 values that a structure can adopt is not well defined, but it appears to be large. An alternative explanation for values which apparently differ markedly from the ideal would be that the sample is partly amorphous, and that the crystalline component of the sample has a composition different to that of the bulk, and hence an ideal c_1/c_2 ratio that differs from the anticipated value. However, electron microscopy has never revealed any evidence in support of this explanation. The anisotropic peak broadening apparent in the FWHM data in Table 2 does suggest that our sample of $Ba_6Mn_4PdO_{15}$ is partially disordered, on the X-ray distance scale, along [001] and we take this to indicate the presence of stacking faults in the layer sequence. The comparable data on $Ba_7Mn_5PdO_{18}$ suggest that this is a highly crystalline sample; the electron diffraction patterns (Fig. 5 and 6) show that the two samples are equally crystalline over the shorter length scale sampled by an electron beam. The observation of $c_1/c_2>1.7$ in $Ba_7Mn_5PdO_{18}$ is in accord with a prediction made previously,[15] namely that high values of this ratio are most likely to be obtained using a cation, for example Mn^{4+}, which is known to be stable in the 2H structure rather than a cation, for example Ir^{4+}, which, as exemplified by the 9R structure of $BaIrO_3$,[23] is not.

The value of the high-temperature Curie constant listed in Table 3 for $Ba_5Mn_3PdO_{12}$ is in good agreement with that predicted using the spin-only magnetic moment of Mn^{4+} ($S=3/2$, $C=1.875\ cm^3\ K\ mol^{-1}$ per Mn^{4+}) and assuming that Pd^{2+} adopts a low-spin ($S=0$) state, as would be expected in square-planar geometry. This agreement can be taken as evidence that the Pd^{2+} cations occupy the trigonal prisms in the $Ba_5Mn_3PdO_{12}$ structure, but that they move away from the ideal site on the 3-fold axis and towards one of the rectangular faces of the prism, thus achieving 4-coordination; similar displacements have been observed in related compounds.[17] However, the values of the Curie constant determined for $Ba_6Mn_4PdO_{15}$ and $Ba_7Mn_5PdO_{18}$ lie closer to those calculated assuming that Pd^{2+} is also paramagnetic with $S=1$. This could be interpreted as evidence that the Pd^{2+} cations lie at the centre of the prismatic site, or that they occupy octahedral sites, with Mn^{4+} cations moving into the prisms. However, the large, negative values deduced for the Weiss constants (Table 3) imply that strong intercation interactions are present in these compounds throughout the measured temperature range, and it is possible that these interactions are strong enough to render the Curie–Weiss law, and hence the detailed interpretation of Curie constants, inappropriate for these compounds below 300 K. Attempts to model the magnetic susceptibility of $Ba_6Mn_4PdO_{15}$ in terms of isolated tetramers gave reasonable agreement with the experimental data at high temperatures. However, the susceptibility of a tetramer in which the superexchange interactions are antiferromagnetic is expected to decrease to zero at low temperatures, and the model is thus incompatible with the increasing susceptibility observed experimentally. The data in Fig. 7 are qualitatively very similar to those recorded for 2H $BaMnO_3$ (the $n=0$ $(A_3A'O_6)_n(A_3O_9)$ phase) by Christensen and Ollivier.[24] No phase transition was apparent in the susceptibility of their sample, which continued to rise with decreasing temperature throughout the range $3<T/K<270$, but neutron diffraction data lead them to suggest that one dimensional magnetic ordering might be occuring along [001] chains at temperatures below 150 K, with a Néel temperature for three dimensional ordering at 2.4 K. It is possible that our samples are showing similar behaviour with the onset temperature reduced to ≈ 100 K by the introduction of Pd^{2+}. Neutron diffraction experiments could confirm this hypothesis, but it would perhaps be difficult to synthesize sufficiently large, homogeneous samples. Furthermore, the analysis of the magnetic structure would be made more difficult by the incommensurate nature of the crystal structure.

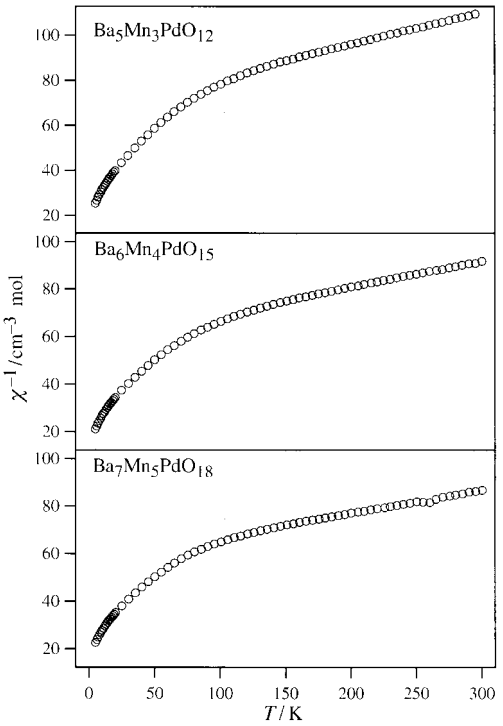

Fig. 7 Temperature dependence of the inverse molar magnetic susceptibility of $Ba_5Mn_3PdO_{12}$, $Ba_6Mn_4PdO_{15}$ and $Ba_7Mn_5PdO_{18}$ measured in 1000 G after ZFC.

In conclusion, we have shown that Pd can be introduced into this structural family, although the resulting compounds are incommensurate and must be considered as composite crystal structures. The most successful demonstration of the stability of the Pd-containing phases is provided by the preparation of $Ba_7Mn_5PdO_{18}$, which resulted in a highly crystalline, monophasic product. This is the first observation of the 14 layer $(p,q)=(7,12)$ member of the structural family. In the case of $Ba_5Mn_3PdO_{12}$ there is evidence to suggest that, although the 2H-related crystal structure is retained, compositional variations occur within the sample. There is no evidence to suggest that inhomogeneities are present in the sample of $Ba_6Mn_4PdO_{15}$, although the width and anisotropic broadening of the X-ray diffraction lines suggest that the crystallinity is relatively low. The fact that only one of our three syntheses has produced a high-quality sample illustrates the difficulties endemic in this area of solid state chemistry. A more extensive program of electron microscopy might facilitate a more detailed characterisation of the microstructure of the other two samples, although it would be difficult to achieve a description of the complexities present, particularly in the case of $Ba_5Mn_3PdO_{12}$, that was sufficiently complete and accurate to serve as the basis for a more detailed study of their electronic properties. The structures drawn in Fig. 2 are likely to be a reasonable representation of these materials, but single-crystal samples suitable for X-ray diffraction will have to be prepared before the details of the structure can be elucidated. The magnetic properties are qualitatively similar to those of 2H $BaMnO_3$, and the differences can be considered to arise from the introduction of Pd^{2+} cations into the magnetic chains.

Acknowledgments

We are grateful to the British Council and the French Ministère des Affaires Etrangères for financial support under the Alliance

programme, and to the EPSRC for the award of a studentship to EJC.

References

1 F. Abraham, S. Minaud and C. Renard, *J. Mater. Chem.*, 1994, **4**, 1763.
2 P. D. Battle, G. R. Blake, J. Darriet, J. G. Gore and F. Weill, *J. Mater. Chem.*, 1997, **7**, 1559.
3 J. Campá, E. Gutiérrez-Puebla, A. Monge, I. Rasines and C. Ruíz-Valero, *J. Solid State Chem.*, 1996, **126**, 27.
4 R. Christoffersen, A. J. Jacobson, S. L. Hegwood and L. Liu, *Mater. Res. Soc. Symp. Proc.*, 1997, **453**, 153.
5 C. Dussarrat, J. Fompeyrine and J. Darriet, *Eur. J. Solid State Chem.*, 1995, **32**, 3.
6 S. Frenzen and H. Müller-Buschbaum, *Z. Naturforsch. Teil B*, 1995, **50**, 581.
7 J. L. Hodeau, H. Y. Tu, P. Bordet, T. Fournier, P. Strobel and M. Marezio, *Acta Crystallogr., Sect. B*, 1992, **48**, 1.
8 M. Neubacher and H. Müller-Buschbaum, *Z. Anorg. Allg. Chem.*, 1992, **607**, 124.
9 T. N. Nguyen, D. M. Giaquinta and H. C. zur-Loye, *Chem. Mater.*, 1994, **6**, 1642.
10 H. Fjellvåg, E. Gulbrandsen, S. Aasland, A. Olsen and B. C. Hauback, *J. Solid State Chem.*, 1996, **124**, 190.
11 J. Darriet and M. A. Subramanian, *J. Mater. Chem.*, 1995, **5**, 543.
12 J. J. Lander, *Acta Crystallogr.*, 1951, **4**, 148.
13 J. R. Randall and L. Katz, *Acta Crystallogr.*, 1959, **12**, 519.
14 M. Huvé, C. Renard, F. Abraham, G. Van Tendeloo and S. Amelinckx, *J. Solid State Chem.*, 1998, **135**, 1.
15 G. R. Blake, J. Sloan, J. F. Vente and P. D. Battle, *Chem. Mater.*, 1998, **10**, 3536.
16 T. N. Nguyen, P. A. Lee and H.-C. zur-Loye, *Science*, 1996, **271**, 489.
17 P. D. Battle, G. R. Blake, J. Sloan and J. F. Vente, *J. Solid State Chem.*, 1998, **136**, 103.
18 A. Tomaszewska and H. Müller-Buschbaum, *Z. Anorg. Allg. Chemie*, 1993, **619**, 534.
19 F. Grasset, F. Weill and J. Darriet, *J. Solid State Chem.*, 1998, **140**, 194.
20 W. T. A. Harrison, S. L. Hegwood and A. J. Jacobson, *J. Chem. Soc., Chem. Commun.*, 1995, 1953.
21 T. Shishido, K. Ukei and T. Fukuda, *J. Alloys Comp.*, 1996, **237**, 89.
22 K. Ukei, A. Yamamoto, Y. Watanabe, T. Shishido and T. Fukuda, *Acta Crystallogr., Sect. B*, 1993, **49**, 67.
23 A. V. Powell and P. D. Battle, *J. Alloys Compd.*, 1996, **232**, 147.
24 A. N. Christensen and G. Ollivier, *J. Solid State Chem.*, 1972, **4**, 131.

Paper 8/05935G